ACS APPLIED MATERIALS & INTERFACES

Research Article

www.acsami.org

Structure-Modified Stress Dynamics and Wetting Characteristics of Carbon Nanotubes and Multilayer Graphene for Electron Field Emission Investigations

Himani Sharma,*[,†,‡] Dinesh C. Agarwal,[§] M. Sharma,[⊥] A. K. Shukla,[†] D. K. Avasthi,[§] and V. D. Vankar[†]

[†]Thin Film Laboratory, Department of Physics, Indian Institute of Technology Delhi 110016, India

[‡]Department of Electrical & Computer Engineering, University of Alberta, 9107 − 116 Street, Edmonton AB T6G 2V4, Canada

[§]Inter University Accelerator Centre, Aruna Asaf Ali Marg, New Delhi 110067, India

[⊥]Agency for Science, Technology and Research (A*STAR), Institute of Materials Research and Engineering, 3 Research Link, Singapore 117602

Supporting Information

ABSTRACT: In the present work, feasibility of achieving enhanced electron field-emission properties of stress-induced carbon nanotubes (CNTs) and multilayer graphene (MLGs) by ion modification is studied. Micro-Raman spectroscopy is used as a potent technique for in-depth investigations of stress-induced CNTs and MLGs. It is found that iron used as a catalyst, compresses at particular fluence and induces stresses in CNTs and MLGs to modify these structures, supported by high-resolution transmission electron microscopy (HRTEM) studies. The stresses are explained by the buckling wavelength ($\lambda \propto e^{(r/t)0.5}$). Furthermore, the stresses induced in exotic nanostructures are studied for investigating wetting properties, which are well-corroborated with electron emission characteristics. It is found out that less-wetted CNTs and MLGs display enhanced emission properties with turn-on voltages (E_{on}) of 1.5 and 2.1 V/μm, respectively, in comparison to hydrophilic CNTs and MLGs with E_{on} of 2.6 and 4 V/μm, respectively.

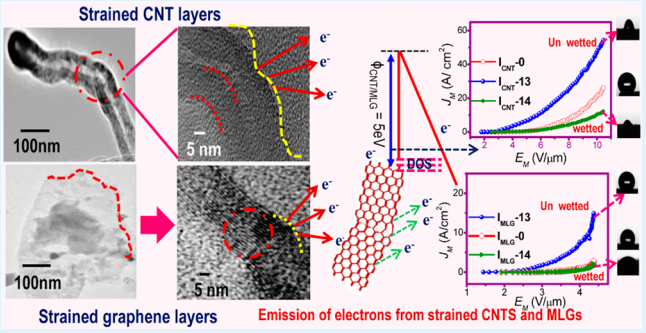

KEYWORDS: *electron field emission, multilayer graphene, carbon nanotubes, structure modification, wettability, micro-Raman spectroscopy*

1. INTRODUCTION

The progress of the carbon-based nanostructures such as graphene and carbon nanotubes (CNTs) for various advanced technological applications including vacuum electronics, nanoelectronics, and field-emission display devices are based on the methods to modify these carbon nanosystems with definitiveness.[1−4] Various methods such as grafting, doping, functionalization, and mechanical strain have been used to modify these unique structures for electron field applications.[5−9] Apart from these methods, the modification by ions is one such method that can be employed for precise alteration and tailoring of CNTs and graphene, resulting in some beneficial effects.[10] The intensive research on irradiation effects in these unique carbon nanostructures is worthwhile, because of their intriguing structural, mechanical, and electronic properties. In our earlier studies, ion irradiation has been explored as a tool to tailor the structure and electron emission properties on CNTs and multilayer graphene (MLGs) as a function of wall thickness.[10] Structural modifications by ion irradiation introduce defects that incorporate in CNTs and graphene are mainly vacancies, interstitial-vacancy pairs, adatoms, and Stone−Wales (SW) defects and intershell covalent bonds that may affect bonding between the carbon atoms. The carbon atoms in both CNTs and graphene form sp^2 and sp^3 bonds, thus making it plausible to observe similar effects after irradiation.[11,12] The defects introduced in CNTs and graphene affect bonding between carbon atoms and induce stresses in carbon bonds and lattices that may eventually affect their structural and, hence, electron emission properties. Micro-Raman and high-resolution transmission electron microscopy (HRTEM) are among the most effective tools to study such effects on modified CNTs and graphene.

The irradiation-induced axial strains and buckling behavior in Ni-filled CNTs were studied by Misra et al., using 100 MeV Au^{7+} ion irradiation.[13] They reported that irradiation of Ni-encapsulated MWCNTs resulted in the lattice damage in both Ni and CNTs. Furthermore, localized amorphous region appears in Ni, whereas planar defects are dominant in the

Received: April 22, 2014
Accepted: July 8, 2014
Published: July 8, 2014

graphite walls of CNTs. The systematic studies of the interaction of 2 MeV protons with monolayer and few-layer graphene was carried out by Mathew et al. and explained that the stability of graphene increases with an increasing number of graphene layers and points toward the role of interaction along the third dimension in stabilizing the quasi-two-dimensional graphene.[14,15] The strains and buckling in carbon bonds and lattices of CNTs and graphene due to irradiation, as mentioned, affect their structural and morphological properties. The tailored geometrical properties in these CNTs and graphene also affect their wettability.[16,17] The wettability of material is dictated by it as surface chemistry and geometrical structure of solid surface and these properties depend on the surface area, surface energy, and surface roughness of these structures.

The structural amendment in carbon nanostructures is well-related to the electron field emission properties. The electron field-emission current depends upon the enhancement factor, which further depends on the geometrical structure and morphology of carbon nanostructures. The electron field properties of stress-induced and wetted carbon nanotubes and graphene is investigated in the present study. The stress-induced in wondorous CNTs and graphene affects the wetting properties and, hence, electron field-emission properties. The stresses in graphene and CNTs are imaged through HRTEM and well-corroborated with micro-Raman studies. Furthermore, we report that surfaces of CNT and MLG can switch to super hydrophilicity under ion irradiation using contact angle measurements and hence results in in electron field emission properties. To the best of our knowledge, electron field-emission properties of stress induced wetted CNTs and MLGs under ion bombardment are not reported so far.

2. EXPERIMENTAL SECTION

The CNT and MLG samples were prepared on Si/SiO_2 substrates using a microwave plasma-enhanced chemical vapor deposition system (MPECVD), described elsewhere.[18−20] Iron (Fe) was used as a catalyst with the thickness of 20 and 50 nm, respectively. The Fe-coated substrates were placed inside the vacuum chamber of the MPECVD system and pretreated in the presence of argon (Ar) and hydrogen (H_2) plasma for 15 min at 550 W. Two sets of samples namely, CNTs and MLGs were investigated further for irradiation effects.

2.1. High Energy Irradiation Using Ag^+ Ion on CNTs and MLGs. The high energy irradiation experiments on CNTs and MLGs were carried out using 100 MeV silver (Ag) ion beam provided by the IUAC Pelletron accelerator. These studies were carried out at different fluences varied from 3×10^{10} to 1×10^{14} ions/cm^2 for both samples. On the basis of irradiation, the samples are named as follows. CNT sample series are named as I_{CNT}-0 (without irradiation), $3I_{CNT}$-10 (3×10^{10} ions/cm^2), I_{CNT}-11 (1×10^{11} ions/cm^2), $3I_{CNT}$-11 (3×10^{11} ions/cm^2), I_{CNT}-12 (1×10^{12} ions/cm^2), I_{CNT}-13 (1×10^{13} ions/cm^2), and I_{CNT}-14 (1×10^{14} ions/cm^2). I_{MLG} samples series are also named in a similar way.

2.2. Characterizations. The microstructures of the samples were imaged using a high-resolution transmission electron microscope (HRTEM) using JEM 2100F and Technai G^2 20 S-Twin model systems. The selected area electron diffraction (SAED) studies of both un irradiated and irradiated CNT and MLG samples were carried out using the G^2 20 S-Twin model operated at 200 kV. A micro-Raman system (Jobin Yvon, Model T64000 triple monochromator) was used to investigate the structures of pristine and irradiated CNTs and MLGs, using an excitation source of 514.5 nm. The diameter of the focused laser spot was ∼1−2 μm. The system is equipped with a charge-coupled device detector and stage movement. Stress-induced in CNTs and MLGs were calculated using micro-Raman spectroscopy.

The wetting properties of CNTs and MLGs were investigated by contact angle (CA) measurements using Krüss DSA30 drop shape analysis system. The CA measurements were performed by placing a drop of deionized water (DI) with a dispensing needle on the various samples used. The wetting angles were measured using a goniometer equipped with a CCD camera and a microscope. A sessile drop was formed over the samples by fixing the needle while approaching toward the sample. The drop was illuminated from one side and a CCD camera at the opposite side records an image of the drop. The BET surface area was measured using a Quantachrome Model Nova 1000 system.

2.3. Electron Field-Emission Properties of Modified CNTs and MLGs. Electron field-emission characteristics of CNTs and MLGs were investigated using a diode setup in the vacuum chamber at a base pressure of 2×10^{-6} Torr. CNT and MLG samples were used as cathode and stainless steel plate was used as anode. The distance between cathode and anode was 250 μm. The measurements were carried out using a high-voltage dc power supply (H5KO2N) and current meter (Keithley 196 system DMM). Electron field-emission characteristics were analyzed using the Fowler−Nordheim (F−N) equation, which is given by[18,21]

$$J_M \approx \lambda_M a \phi^{-1} \gamma_C^{\ 2} E_M^{\ 2} \exp\left(- \frac{\nu_F b \phi^{3/2}}{\gamma_C E_M} \right) \quad (1)$$

Here, J_M is the macroscopic current density, E_M the macroscopic field, λ_M a macroscopic pre-exponential correction factor, and ν_F the correction factor; $a = 1.54 \times 10^{-6}$ A eV V^{-2} and $b = 6.83 \times 10^7$ eV$^{3/2}$ V cm^{-1}.

Equation 1 is the full barrier equation for large-area field emitters. Here, ϕ is the work function and γ_C is a macroscopic field-enhancement factor.

3. RESULTS AND DISCUSSION

3.1. HRTEM Studies of Modified CNTs and Graphene. The HRTEM images of pristine MWCNTs and MLG structures are shown in panels a and b in Figure 1. The inset images in the corresponding images show the SAED pattern of CNTs (002) planes and graphene (0001) planes with a d-spacing of ∼0.34 nm. In our previous work, it is reported that the diameter of MWCNTs (number of walls) and thickness of graphene (number of layers) depends on the thickness of the catalyst (Fe) layer.[18] As the thickness of Fe is increased (≥50 nm) bigger nanoclusters of Fe form and help in the condensation of carbon to form graphene. Here, in Figure 1a, the diameter of MWCNTs corresponds to ∼30 nm and the thickness of graphene flakes is ∼50 nm. Figures 1c and 1d show the images corresponding to the samples I_{CNT}-13 and I_{MLG}-14 samples. The changes were insignificant, that were observed, after irradiation at low fluences (not shown here). In the earlier studies, it is mentioned that, at low fluences, the walls of CNTs and graphene layers get modified.[10] However, at higher fluences (1×10^{13} ions/cm^2) damages prevail in the structure. The arrows and marks in Figure 1c shows the damage and breaking of bond at the higher fluence. The entanglement of the graphene layers is clearly seen in Figure 1d at the fluence of 1×10^{14} ions/cm^2.

The most common defect in MWCNTs is intershell covalent bond that is formed by the two dangling bonds at the vacancies in the adjacent shell.[4] These dangling bonds can be energetically saturated by the vacancy and the interstitial carbon, leading to modification in the MWCNTs. After carrying out the irradiation studies for all ion fluences, it is observed that I_{CNT}-12 and I_{MLG}-12 show modification in their structures, which has been confirmed by HRTEM and micro-Raman analysis. At lower fluences, the carbon atoms are

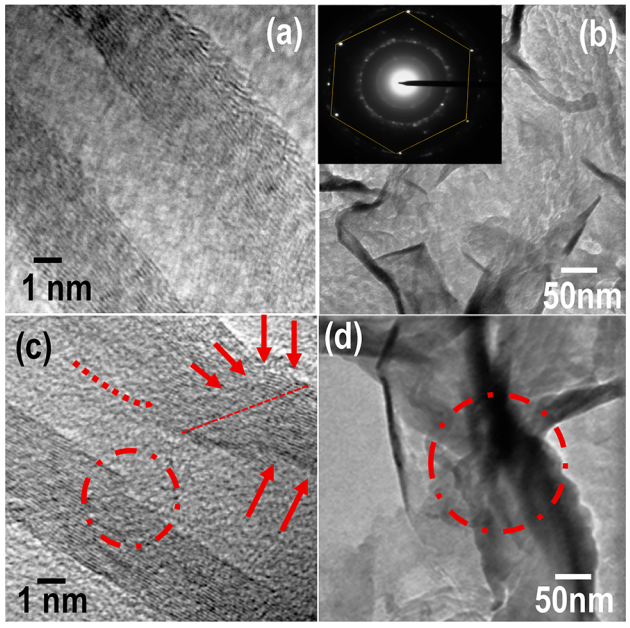

Figure 1. HRTEM images of MWCNTs and MLGs without ion modification: (a) I_{CNT}-0, (b) I_{MLG}-0 (inset image displays a selective-area diffraction pattern from MLGs and confirm the graphene structure); MWCNTs and MLGs with ion modification (c) I_{CNT}-13 and (d) I_{MLG}-14. Here, "0" corresponds to the as-prepared CNTs and MLGs. I_{CNT}-13 and I_{MLG}-14 correspond to CNTs and MLGs modified at a fluence of 1×10^{13} ions/cm^2 and 1×10^{14} ions/cm^2, respectively.

displaced from their position causing vacancies at the side walls. At mid-fluences, the side wall vacancies bond together to satisfy the unsaturated bonds, a process that heals the system. The defects and healing mechanisms are explained by the bending in CNTs and reorganizations of bond in graphene layers.

Figures 2a and 2b show the bending in CNT walls for I_{CNT}-12 samples, respectively. On irradiation, displacement of carbon atoms leads to new bond formations and results in healing CNTs. The carbon atoms get removed from the MWCNTs locally, as seen in Figures 2c and 2d, which leads to formation of vacant sites. The images are taken for bamboo-shaped CNTs at a fluence of 1×10^{12} ions/cm^2 taken at different magnifications. Because of the large number of walls, the inner walls start to bend as the carbon atoms are removed from the outer shells. The bending in inner walls is related to the formation of vacancies in the outer shells. These vacancies created because of irradiation are immobile and thus cause tapering in the inner walls. The bending in the inner walls leads to rearrangement of carbon atoms via the formation of new bonds, thereby modifying the carbon system.[22]

The rearrangement of carbon bonds in MLGs are shown in images e and f in Figure 2. A structural modification by tapering and bending in CNTs and MLGs is shown using the schematic illustrations in Figures 2g–i that suggest the displacement of carbon atoms and the new bond formations can be a result of healing mechanism in CNTs. The structure of graphene has an ability to reconstruct its lattice around intrinsic defects, leading to interesting effects.[23] The shaded region shows that the carbon atoms at the edges are affected more on irradiation in comparison to the carbon atoms at the center of the layer. These carbon atoms rearrange to form new bonds and stabilize

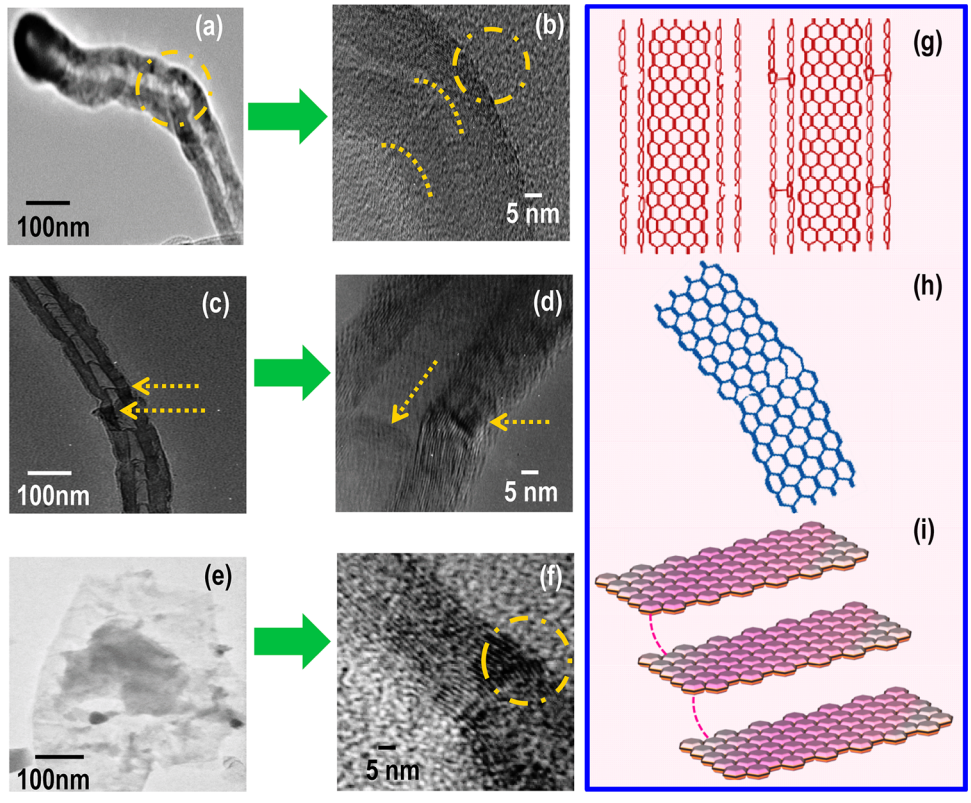

Figure 2. Structure modification through bending is displayed through HRTEM of CNTs and MLG planes: (a, b) CNTs at a fluence of 1×10^{12} ions/cm^2 (I_{CNT}-12), (c, d) I_{CNT}-12 on bamboo-shaped CNTs at different magnifications, (e, f) I_{MLG}-12. The marks and arrows illustrate the modified area by ion irradiation. (g, h, i) Schematic illustration of modification and healing in carbon nanostructures.

dx.doi.org/10.1021/am502405n | ACS Appl. Mater. Interfaces 2014, 6, 12531–12540

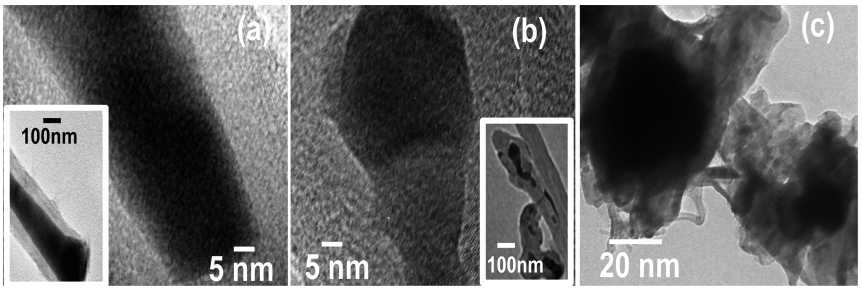

Figure 3. Effect of ion irradiation on Fe catalyst is shown in the HRTEM images. (a) Growth of Fe as a nanorod grown in parallel to CNT planes; inset shows Fe catalyst at low magnification. Effect of ion irradiation on the shape of Fe catalyst is shown in (b) CNT and (c) MLG samples.

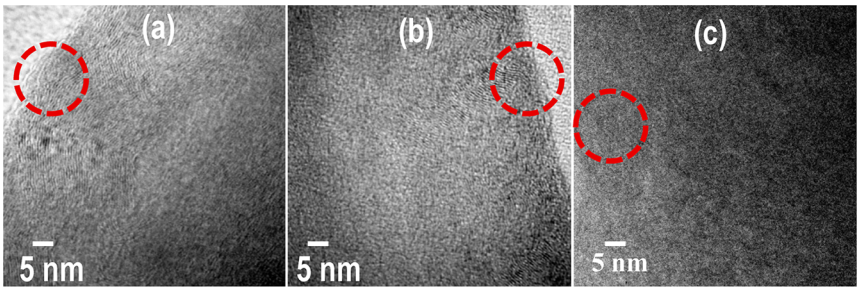

Figure 4. (a) Outward buckling of CNT walls is shown by HRTEM image of CNTs (I_{CNT}-13 sample), resulting in stressed planes; amorphization at higher fluence for (b) CNTs (I_{CNT}-14 sample) and (c) MLG (I_{MLG}-14 sample). The carbon nanostructures buckle outward and amorphize at higher fluencies.

the energy of the system. Ion irradiation on CNTs and MLGs samples also affects Fe nanoparticle that is used as a catalyst for the growth of these structures. The Fe catalyst grows like a nanowire along with CNTs as shown in HRTEM image of I_{CNT}-0 (Figure 3a). The inset image shows the same image at low magnification. It can be seen that CNTs are grown without any buckling in the sidewalls and is grown vertically. It is seen from HRTEM images that the walls look perfectly crystalline with the *d*-spacing of CNTs lattice planes being ∼3.4 Å and that for Fe lattice planes being ∼2.1 Å. Upon irradiating carbon nanostructures at a fluence of 3×10^{11} ions/cm^2, the Fe catalyst also gets stressed. The stresses in the Fe catalyst consequently stress the CNT walls, as observed in Figure 3b.

The compressed nanorod of Fe after irradiation shows the *d*-spacing of lattice planes to be ∼1.8 Å and *d*-spacing for CNTs resulted to be ∼3.1 Å. This difference in lattice *d*-planes results that crystalline planes of CNTs and Fe catalyst are compressed under irradiation. However, in the case of MLGs, the layers are completely compressed and become damaged after irradiation, as seen in Figure 3c. The image is taken at a fluence of 1×10^{13} ions/cm^2 for the MLG sample. In earlier studies on nickel-encapsulated CNTs by Misra et al., they have explained the expansion of nanorods along with the buckling of MWCNTs on irradiation by Au^+ ions on the basis of a thermal spike model.[13,24]

Figure 4 shows the HRTEM images of I_{CNT}-13, I_{CNT}-14, and I_{MLG}-14 samples at higher fluencies. Their corresponding autocorrelated images are shown in Figure S1 in the Supporting Information. As explained earlier, CNTs buckle outward to lose their crystallinity. The expanded walls can be seen in Figure 4a at a fluence of 1×10^{13} ions/cm^2. However, the walls are almost amorphized at a fluence of 1×10^{14} ions/cm^2, resulting in bond rupture of the CNT structure. The encircled portions in the images display the modified and amorphized regions (Figure 4c). Similarly, graphene sheets in MLGs deteriorate at a fluence of 1×10^{14} ions/cm^2, as observed in Figure 4c.

At such high fluences, these unique carbon nanostructures amorphize completely and no healing is observed, as seen in the autocorrelated images shown in Figures S1a–d in the Supporting Information.

3.2. Stress Dynamics Behavior Using Micro-Raman Studies on High-Energy-Irradiated CNTs and MLGs. The strains/stresses in CNT and graphene walls through irradiation, as seen through HRTEM studies, are well-correlated with micro-Raman spectroscopy. Micro-Raman spectroscopy is a powerful technique to investigate the defects, crystallinity, and strains present in carbon-based structures.[25,26] Micro-Raman spectra of I_{CNT}-0 and I_{MLG}-0 samples, irradiated at different fluences, are shown in Figure 5. The main peaks in the spectra are D-mode (1355 cm^{-1}), G-mode (1580 cm^{-1}), and 2D-mode (2700 cm^{-1}). D-mode corresponds to the defects present in CNTs and graphene and points to the *K*-position in the Brillioun zone.[26] The G-mode corresponds to the graphitic nature of CNTs and graphene points to the Γ-position with E_{2g} symmetry in the Brillioun zone. The 2D-mode is the signature of the presence of graphene and is a result of double resonance phenomenon between the *K*-points in the Brillioun zone. The ratio of the D-mode to the G-mode (I_D/I_G) provides the order of defects in CNTs and ratio of the 2D-mode to the G-mode (I_{2D}/I_G) estimates the number of layers in graphene. The peak positions are mentioned in Table 1. Figure 5a shows the first-order Raman spectra of I_{CNT} sample. The order of defects (I_D/I_G) varies with the ion fluence. The I_D/I_G value for the I_{CNT}-0 sample is 0.8. The I_D/I_G value for all samples was averaged over three plots. As the ion fluence increases from 3×10^{10} ions/cm^2 to 1×10^{11} ions/cm^2, the defects comes into play, confirmed by the increase in I_D/I_G value to 1.07 (0.04). Furthermore, upon increasing the ion fluence to 3×10^{11} ions/cm^2, the I_D/I_G value is observed to be nearly the same as that for 1×10^{11} ions/cm^2

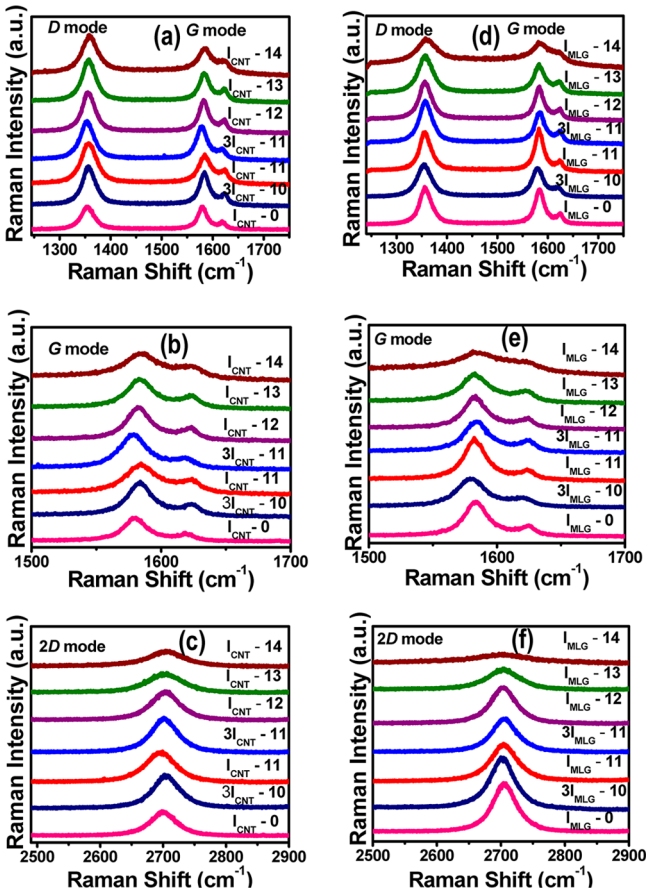

Figure 5. Stress-induced studies in CNTs and MLGs are shown by micro-Raman spectra: (a–c) CNT samples ((a) D- and G-modes, (b) characteristic G-mode for CNTs, (c) characteristic 2D-mode, shown at different fluences for all CNT samples); and (d–f) MLG samples ((d) D- and G-modes, (e) G-mode for MLGs, and (f) characteristic 2D-mode, shown at different fluencies for all the MLG samples). Micro-Raman is also used to investigate the crystallinity of MLGs samples before and after ion irradiation at different fluences. Micro-Raman is also used to investigate the crystallinity of CNTs and MLG samples before and after ion irradiation at different fluences.

(0.1), indicating that the defects are persistent. Furthermore, at higher fluences (1×10^{12} to 1×10^{14} ions/cm^2), the order of defects increases in comparison to 3×10^{11} ions/cm^2, confirming disorders in the system at higher fluences. The peak position of the G mode for I_{CNT}-0 sample corresponds to 1580.2 cm^{-1}, shown in Figure 5b. Upon irradiation with a fluence of 3×10^{10} ions/cm^2, the G-mode blue-shifts to 1583.2 cm^{-1} for the I_{CNT}-0 sample (Table 1). Furthermore, at a fluence of 1×10^{11} ions/cm^2 for the same sample, the G-mode peak attains a position at 1584.1 cm^{-1}. A shift in the peak position is related to the stresses induced in the structure; a blue shift (phonon hardening) in the peak at lower fluences corresponds to compressive stresses in CNTs.[27,28] It is mentioned that defects in MWCNTs are mainly intershell covalent bonding.[29] The stress incorporated phonon hardening may be related to the compressive stresses in the outer walls. At lower fluences, only the outer walls are affected by defects, the result of which shifts the G-mode peak toward higher wavenumbers. At the middle range of ion fluence (3×10^{11} ions/cm^2), the G-mode red-shifts (phonon softening) to 1580.1 cm^{-1}.

This position is nearly same as that of the I_{CNT}-0 sample. This lower wavenumber shift may be related to the stretching, weakening, and formation of new C–C bonds in CNTs, causing bending in the inner walls, as shown in HRTEM studies. Thus, displaced carbon atoms at lower fluences try to bond again with the unsaturated carbon atoms at middle ion fluences and may result in stretching. In MWCNTs, defect saturation may occur by migration of interstitial atom and unsatisfied surface bond saturation forming intertube covalent bonds. On further impinging MWCNTs at higher fluences (1×10^{12} ions/cm^2 and 1×10^{13} ions/cm^2), the G-mode peak is found again to blue-shift to higher wavenumbers. The maximum shift in the G-mode peak (1585.1 cm^{-1}) is found at a fluence of 1×10^{14} ions/cm^2 in comparison to the I_{CNT}-0 sample (1580.2 cm^{-1}). Damage in CNT structures due to irradiation also affects the D-mode. A drastic variation is seen in the D-mode peak from 1355 cm^{-1} (I_{CNT}-0) to 1352 cm^{-1} (I_{CNT}-14), confirming the deterioration in CNTs. Similar to G-mode, phonon hardening is also seen in 2D-mode, from 2700.3 cm^{-1} to 2705.8 cm^{-1} for the I_{CNT}-0 and I_{CNT}-14 samples, respectively (Figure 5c). The 2D-peak follows the same trend as that of the G-mode. At higher fluences (1×10^{12} ions/cm^2 to 1×10^{14} ions/cm^2), defects are more pronounced to cause the damage in MWCNTs. The intertube covalent bonds between interstitial carbon atom and surface carbon atoms are aggressive enough to damage the CNTs at higher fluences. It can be seen from the Raman spectra, all D-, G-, and 2D-modes become broader and dampen at higher ion energies. The broadening in the D-, G-, and 2D-modes can be estimated through line-width values, as mentioned in Table 1. It is seen that the line width varies as 26.5 cm^{-1} (I_{CNT}-0) to 31 cm^{-1} (I_{CNT}-14) for D-mode, 25 cm^{-1} (I_{CNT}-0) to 28 cm^{-1} (I_{CNT}-14) for G-mode and 42 cm^{-1} (I_{CNT}-0) to 47 cm^{-1} (I_{CNT}-14) for 2D-mode.

This phonon hardening directs toward the compressive stresses in CNTs. From Raman studies on CNT samples, it is found that irradiation at lower energy (1×10^{10} ions/cm^2 and 3×10^{11} ions/cm^2) builds up compressive stresses in CNTs. However, at the middle of the ion fluence, CNTs attains the same behavior as that of unirradiated CNTs followed by building of tensile stresses (1584.1 to 1580.1 cm^{-1}) again at higher fluence (1×10^{12} to 1×10^{14} ions/cm^2).

A reverse trend is observed for MLG (I_{MLG}-0) samples, as shown in Figures 5d–f. Figure 5d shows the first-order Raman spectra of I_{MLG} samples. It is observed that phonon softening occurs for G- and 2D-mode at lower fluences (Figures 5e and 5f). At higher fluences, phonon hardening is observed for the same Raman active modes. Figure 5 and Table 1 indicate that the D-, G-, and 2D-modes for the I_{MLG}-0 and I_{MLG}-14 sample shift to lower wave numbers (1356 to 1354 cm^{-1}, 1583.8 to 1581.1 cm^{-1}, and 2705.3 to 2702.5 cm^{-1}, respectively). In the case of MLGs, I_D/I_G values are found to be statistically the same (Table 1). However, the damage in the structure can be verified by variation in I_{2D}/I_G and HRTEM results at 1×10^{14} ions/cm^2. The I_{2D}/I_G ratio, which is an important parameter for MLGs, shows values from 1.28 to 0.66 for I_{MLG}-0 and I_{MLG}-14 samples, respectively (not shown in the table). Figure 5f also shows that the 2D-mode at a fluence of 1×10^{14} ions/cm^2 almost vanishes, confirming our results. The line-width values of the D-, G-, and 2D-mode peaks for MLGs also provide details about the effect of irradiation on structures by observed broadening in the aforementioned peaks (see Table 1). It is seen that the line width varies as 29.5 cm^{-1} (I_{MLG}-0) to 35 cm^{-1} (I_{MLG}-14) for D-mode, 22 cm^{-1} (I_{MLG}-0) to 29 cm^{-1} (I_{MLG}-14) for G-mode, and 38 cm^{-1} (I_{MLG}-0) to 50 cm^{-1} (I_{MLG}-14) for 2D-mode. It was expected that healing might have taken place,

Table 1. Micro-Raman Parameters of Stress-Induced CNTs and MLGs at Different Ion Fluences

					Full Width at Half Maximum, fwhm (cm^{-1})		
sample series	D-mode (cm^{-1})[a]	G-mode (cm^{-1})[b]	2D-mode (cm^{-1})[c]	I_D/I_G[d] (error)	D-mode	G-mode	2D-mode
			I_{CNT} (CNTs)				
I_{CNT}-0	1355	1580	2700.3	0.8 (0.05)	26.5 ± 0.3	25 ± 0.2	42 ± 0.2
3I_{CNT}-10	1356	1583.2	2704.3	0.96 (0.03)	27 ± 0.3	25.4 ± 0.1	41.5 ± 0.1
I_{CNT}-11	1356	1584.1	2696.3	1.07 (0.04)	27 ± 0.4	26 ± 0.3	43 ± 0.2
3I_{CNT}-11	1354	1580.1	2701.9	1 (0.1)	26.8 ± 0.3	25.3 ± 0.4	42 ± 0.4
I_{CNT}-12	1354	1582.6	2704.29	1.05 (0.03)	27 ± 0.4	26 ± 0.1	43 ± 0.5
I_{CNT}-13	1356	1583.1	2704.9	1.08 (0.05)	29.8 ± 0.5	26.5 ± 0.5	45 ± 0.5
I_{CNT}-14	1352	1585.1	2705.8	1.09 (0.04)	31 ± 0.5	28 ± 0.4	47 ± 0.5
			I_{MLG} (MLGs)				
I_{MLG}-0	1356	1583.8	2705.3	1.0 (0.05)	29.5 ± 0.2	22 ± 0.3	38 ± 0.4
3I_{MLG}-10	1355	1579.7	2702.3	1.04 (0.07)	30.8 ± 0.3	22.5 ± 0.1	41 ± 0.2
I_{MLG}-11	1355	1582.4	2703	0.97 (0.03)	29 ± 0.4	22 ± 0.3	43 ± 0.5
3I_{MLG}-11	1355	1583.1	2704.5	1.1 (0.1)	29.5 ± 0.1	22.8 ± 0.2	39 ± 0.6
I_{MLG}-12	1354	1582.2	2702.7	1.04 (0.04)	29.9 ± 0.1	23 ± 0.1	44 ± 0.3
I_{MLG}-13	1354	1582.2	2702.3	1.05 (0.06)	31 ± 0.5	24 ± 0.2	48 ± 0.4
I_{MLG}-14	1354	1581.1	2702.5	1.07 (0.05)	35 ± 0.6	29 ± 0.5	50 ± 1

[a]D-mode appears at ~1355 cm^{-1} and corresponds to local disorder present. [b]G-mode appears at 1580 cm^{-1} and corresponds to the in plane vibrations of carbon atoms. [c]2D-mode is the second-order Raman mode. [d]I_D/I_G is a ratio between the D-mode and the G-mode, i.e., I_D/I_G is an important tool to estimate the quality of the CNT samples.

because of the shift in the peak position at 3×10^{11} ions/cm^2 and samples acquiring roughly the same positions as that of non-irradiated samples. However, I_D/I_G values and peak width values do not correspond to healing. It may be possible that, above 3×10^{11} ions/cm^2, both healing and damaging processes compete, since healing is apparently not quantitative.

Variation in the peak positions of all the modes (D, G, and 2D) with increasing ion fluences are shown in Figure 6. The defects incorporated and stress variation with change in peak positions of D-, G-, and 2D-modes for CNTs (Figure 6a) and MLGs (Figure 6b) can be estimated through the plots. The difference in the Raman behavior of CNTs and MLGs are due to differences in both the structures. In the rolled carbon cylinders, defects prevail from outer walls and extend to the inner walls. In contrast, in planar sheets, carbon atoms on the edge are easily responsible for defect formation that can be extended by the number of layers. Different ion fluences modify both structures differently, and, hence, the stress behavior through Raman spectroscopy is not similar.

On the basis of Raman studies, stresses acquired by CNTs and MLGs after irradiation were investigated (Figure 7a). As explained from shift in peak position of G-mode, the behavior of stresses is complementary to each other. CNTs are stressed by compressive forces and MLGs are stressed by tensile forces.[30] At one particular fluence (3×10^{11} ions/cm^2), the G-mode peak position acquires the same position as that of a pristine sample for both CNTs and MLGs. Thus, no stresses are acquired at that fluence. The stresses are calculated via the shift in the Raman peak, using the following relation:[31]

$$\omega_\sigma - \omega_o = \frac{A(S_{11} + S_{12})\sigma}{\omega_o} = \alpha\sigma \quad (2)$$

Here, α is the stress coefficient, with a value of 7.47 cm^{-1}/GPa. S_{11} and S_{12} are the graphitic elastic coefficients. ω_o is the G-mode peak value for CNTs and graphene, taken as 1580 or 1581 cm^{-1}. ω_σ is the stress acquitted by carbon nanostructures. A is a constant, having a value of -1.44×10^7 cm^{-2}.

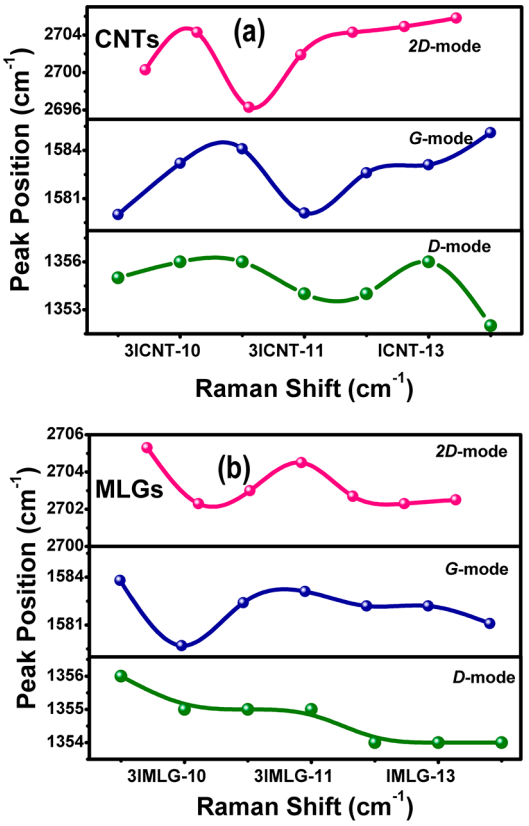

Figure 6. Graphs displaying the variation in peak positions of Raman modes with increasing ion fluence for (a) CNTs (D-, G-, and 2D-modes), (b) MLGs (D-, G-, and 2D-modes).

The relation is used for both CNTs and graphene structures. The reason for that may be the displaced carbon atoms at low fluence join to form new bonds in order to stabilize the energy of the entire system. However, at higher fluences, no stabilization occurs for both CNTs and MLGs. The structures acquire more defects and reveal their respective stresses.

dx.doi.org/10.1021/am502405n | ACS Appl. Mater. Interfaces 2014, 6, 12531−12540

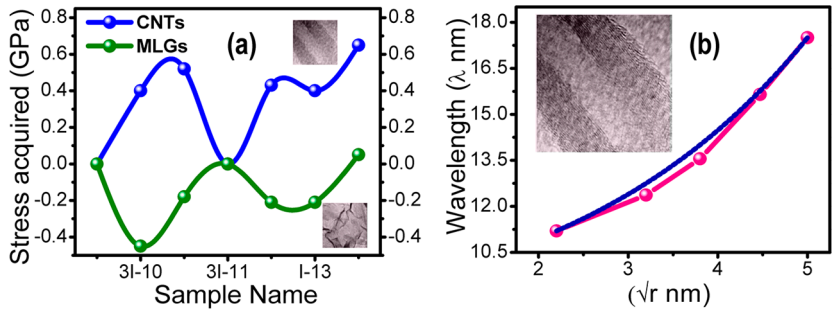

Figure 7. Graphs presenting (a) stresses accumulated in CNTs and graphene post irradiation and (b) relation between buckling wavelength with CNT diameters fitted with $\lambda \propto e^{(r/t)0.5}$.

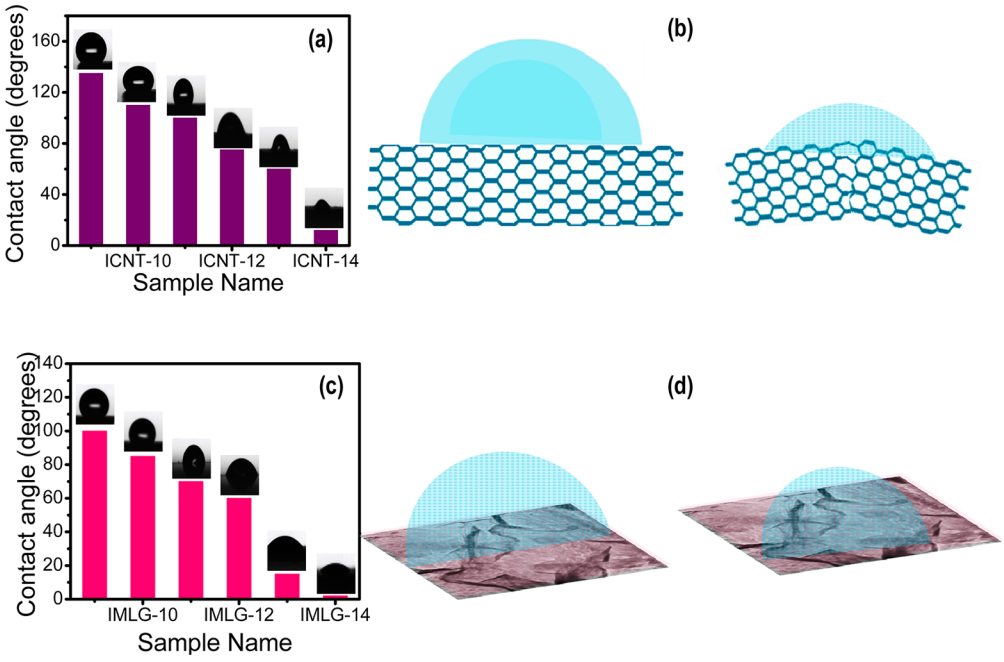

Figure 8. Wetting properties of stress-induced, ion-modified CNTs and MLGs are shown. Statistical distribution of contact angles of ion-modified carbon nanostructures at different fluences and schematic images displaying a change in wetting characteristics of (a, b) CNTs from hydrophobic to hydrophilic and (c, d) MLGs from hydrophobic to superhydrophilic.

The blue shift in CNT samples on irradiation has been explained by the torsional strain and is explained by the relation $\lambda \propto e^{(r/t)0.5}$.[32,33] Here, λ is the buckling wavelength, r is the radius of the CNTs, and t is the thickness of the tubes. Figure 7b shows a plot between buckling of CNTs on irradiation versus their radius.

3.3. Wetting Properties of Irradiation Tailored CNTs and MLGs. Stress-induced CNTs and MLG structures are further characterized for their wetting properties, which is a part of structural investigation. The wettability of a solid by a liquid is characterized in terms of angle of contact between the two. The contact angle (CA) of graphite is 87°, which means that the CNTs and MLGs are difficult to wet. It is reported that the surface free energy of graphene sheets is 46.7 mJ/m^2, thus making it water-repelling. In contrast, graphene oxide exhibits hydrophilic character because of the presence of C−OH with the higher surface energy (62.1 mJ/m^2) in comparison to graphene.[34] Depending on the structure and cohesive bonding between the atoms and molecules, wettability of these carbon-based materials change. The CA distribution of high-energy-irradiated I_{CNT}-0, and I_{MLG}-0 samples are shown in Figure 8a through a histogram. The CA values of these samples are listed in Table S1 in the Supporting Information.

It is observed from HRTEM and micro-Raman studies that irradiation induces modifications in the morphology and, hence, the structure of CNTs and MLGs. The CA measured from 3I_{CNT}-10, I_{CNT}-11, I_{CNT}-12, I_{CNT}-13, and I_{CNT}-14 samples are shown in Figure S2a in the Supporting Information. These images indicate that the CA decreases upon increasing the irradiation dose (from I_{CNT}-0 to I_{CNT}-14 sample). The I_{CNT}-0, 3I_{CNT}-10, I_{CNT}-11, and I_{CNT}-12 samples shows hydrophobic behavior. However, I_{CNT}-13 and I_{CNT}-14 exhibit hydrophilic behavior. These results can be explained using the Wenzel model, which expresses the apparent contact angle on a rough surface:[35,36]

$$\cos \theta_w = r(\cos \theta) \tag{3}$$

where θ is the contact angle on the flat surface and r the roughness ratio is defined as the ratio of the true area of the solid surface to its projected area. Considering $r > 1$, it is inferred that θ_w would be higher than θ in the case of a hydrophobic surface. In the reverse case, the surface will be hydrophilic. The difference in CA from 135° to 12° for I_{CNT}-0

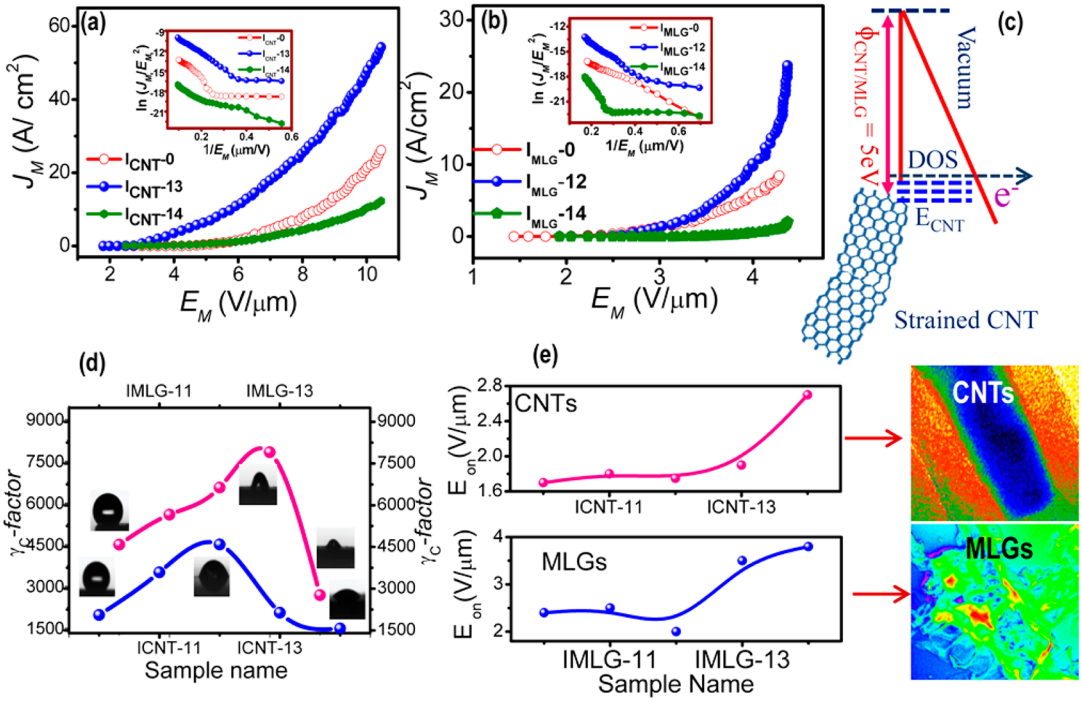

Figure 9. (a) Electron field-emission studies showing variation of macroscopic emission current density (J_M) with macroscopic electric field (E_M) from stress-induced carbon nanostructures for (a) CNTs and (b) MLGs; (c) tunneling of electrons from stress-induced CNTs. Electron field-emission parameters ((d) enhancement factor (with an error value of 0.6% to 0.9%) and (e) turn-on field (E_{on})) are shown for pristine and stress-induced CNTS and MLGs (with an error value of 0.1%−0.2%). Colored TEM images of CNTs and MLGs are shown at the right of panel e, upon which electron field-emission studies were carried out.

and I_{CNT}-14, respectively, is due to the stresses induced in CNTs by structural modification in CNTs, which leads to vacancy formation, breakage of C−C bonds, etc., by ion irradiation, as proved by Raman spectroscopy. As a result of which, the compact structures have space between them, which act as capillaries, and allows the water to seep. Thus, irradiation-modified CNTs have higher surface energy, in comparison to the pristine CNTs. As a result, irradiated CNTs get wetted by water and exhibit hydrophilic or even close to superhydrophilic behavior, as displayed in Figure 8b. The BET surface for few selected samples are found to be 210 m^2/g (I_{CNT}-14) and 390 m^2/g I_{CNT}-14, which is persistent with the change in CA.

The CA behavior of I_{MLG}-0, I_{MLG}-10, I_{MLG}-11, I_{MLG}-12, I_{MLG}-13, and I_{MLG}-14 samples is shown in Figure 8c and Figure S2b in the Supporting Information. The MLG samples with large surface area exhibit hydrophobicity with a CA of 100°. However, the I_{MLG}-0 sample shows smaller CA values, in comparison to that of I_{CNT}-0 sample. Upon irradiation, the CA decreases showing hydrophilic nature for I_{MLG}-10, I_{MLG}-11, and I_{MLG}-12 samples. At higher fluence, I_{MLG}-13 and I_{MLG}-14 samples acquire superhydrophilicity with CA values of 15° and 2°, respectively. It is mentioned that graphene exhibits hydrophobic behavior, because of low surface energy. However, upon irradiation, the sample nature changes to hydrophilic and superhydrophilic. Upon irradiation, MLGs have defects and damaged graphitic planes affect the cohesivity between the carbon atoms. Thus, the weak bonding between the carbon atoms on irradiation results in increased surface energy and increased wetting can be seen in Figure 8d. The BET surface area for I_{MLG}-0 and I_{MLG}-14 are found to be 237 and 412 m^2/g, respectively, and can be related to wettability. We tried to measure the roughness values through atomic force microscopy (AFM). However, because of the quite rougher surface, we could not measure the roughness accurately.

The wetting was affected (although not drastically). However, a change in CA was observed because of the irradiation, even at low fluences. A modification in carbon nanostructures is expected to start at 1 × 10^{11} ions/cm^2 (explained by micro-Raman studies). This corresponds to the local ordering/disordering in the structure. The surface is expected to change not so progressively. However, with the increase in ion fluence, formation of defects, breaking and formation of new bonds is quite progressive to affect the wettability strongly. However, the wetting properties have started to change from first dose of irradiation (1 × 10^{11} ions/cm^2) and effective changes are seen.

3.4. Electron Field-Emission Properties of Stress-Modified CNTs and MLGs. The morphology and geometry of CNTs and graphene have an important role in electron emission properties of CNTs. The structutal modification, stress dynamics, and wetting characteristics of CNTs and MLGs are well-corroborated with their electron field-emission characteristics, shown in Figure 9.

Figures 9a and 9b present the macroscopic emission current density (J_M) versus macroscopic electric field (E_M) characteristics of as prepared (I_{CNT}-0 and I_{MLG}-0) and stress-modified (I_{CNT}-13 and I_{MLG}-12) and deteriorated (I_{CNT}-14 and I_{MLG}-14) CNTs and MLGs, respectively. The F−N plots of the samples are shown in their corresponding inset images. The electron field-emission characteristics for CNTs and MLGs are given by Fowler−Nordheim (F−N) theory, which is described elsewhere.[18,21] The equation is used to calculate the field-enhancement factor (γ_C factor). It is seen that stress-induced CNTs and MLGs show enhanced emission characteristics in comparison to the as-prepared samples. It is deduced from

micro-Raman and HRTEM studies that CNTs and MLGs are modified at a particular fluence because of irradiation that may help in felicitation of electrons from these structures (Figure 9c). However, higher ion fluence damages and amorphizes these carbon-based structures and electron emission properties get deteriorated. The calculated γ_c factor for CNTs and MLGs are shown in Figure 9d. The γ_c factor is a structure- and geometry-based factor and thus correlated with the wetting properties of structure-modified CNTS and MLGs. The γ_c factor value increases for stress-induced CNTs and MLGs for samples I_{CNT}-13 and I_{MLG}-12 and then decreases for samples I_{CNT}-14 and I_{MLG}-14. The maximum value of γ_c factor for I_{CNT}-13 and I_{MLG}-12 samples achieved are 7824 and 4589, respectively. The γ_c factor I_{CNT}-14 and I_{MLG}-14 are 2685 and 1568, respectively, which are the lowest values achieved. Not much change is found in turn-on (E_{on}) field value for I_{CNT}-0, I_{CNT}-12, and I_{CNT}-13 samples, as shown in Figure 8e. The E_{on} values for these samples are 1.7 V/μm. The E_{on} value increases for deteriorated I_{CNT}-14 sample to 2.7 V/μm. However, E_{on} value decreases from 2.4 V/μm for I_{MLG}-0 to 2.0 V/μm for I_{MLG}-12. Furthermore, it is also observed that the CA value is highest for the as-prepared samples, showing hydrophobic character. However, as explained above, as the structure of CNTs and MLGs are modified with an ion fluence of 1×10^{12} ions/cm^2 for CNTS and MLGs, the wetting characteristics change from hydrophobic character to hydrophilic character. As the wetting character changes because of structure modification, electron field-emission properties changes. It is observed that most hydrophilic CNTs and MLGs acquire lower electron field-emission properties. The enhanced electron field-emission properties for I_{CNT}-13 and I_{MLG}-12, in comparison to I_{CNT}-0 and I_{MLG}-0, are found due to local modifications in the structures of CNTs and MLGs that provide the local density of states. These local states, due to morphology and structural changes, effectively modify the local work function and facilitate the emission of electrons.[9,37] Furthermore, for samples I_{CNT}-14 and I_{MLG}-14, as the ion fluence is increased to 1×10^{14} ions/cm^2, the rupture in carbon bonds results in amorphization of the tips, resulting in reduced electron field-emission properties.

4. CONCLUSIONS

It is concluded that irradiation influences and tailors the structure of carbon nanotubes (CNTs) and multilayered graphene (MLGs) and, hence, enhance their electron field-emission properties. HRTEM studies reveal that iron (Fe) grown as nanorod buckles outward during irradiation and induces stresses in CNT and MLG graphitic layers. An exponential relation between buckling wavelength and CNT diameters was used to analyze the buckling in carbon nanostructures. The stresses induced by formation of defects and change in crystallinity were confirmed by micro-Raman spectroscopy. A shift in the G-mode (graphitic) and 2D-modes of CNTs and MLGs results in tensile and compressive stresses, respectively. Furthermore, the structure modifications in CNTs and MLGs are confirmed by wetting studies. It is shown that ion-modified CNTs and MLGs after irradiation at a fluence of 1×10^{14} ions cm^{-2} display the superhydrophilic character with a contact angle (CA) of 12° and 2°, respectively. These results are correlated with electron field-emission studies, and it is found that less-wetted CNTs and MLGs display enhanced emission properties at mid-fluence ranges (1×10^{11} ions cm^{-2}–1×10^{13} ions cm^{-2}). However, because of deterioration in the structure at higher fluences (1×10^{14} ions cm^{-2}), the hydrophilic CNTs and MLGs show poor emission properties.

■ ASSOCIATED CONTENT

Ⓢ Supporting Information

HRTEM results, micro-Raman spectroscopy data, X-ray photoelectron spectroscopy, and contact angle details. This material is available free of charge via the Internet at http://pubs.acs.org.

■ AUTHOR INFORMATION

Corresponding Author

*E-mail: himani@ualberta.ca.

Notes

The authors declare no competing financial interest.

■ ACKNOWLEDGMENTS

The financial support of the Ministry of Information Technology (MIT), Government of India, is gratefully acknowledged for this work.

■ REFERENCES

(1) Chau, R.; Doyle, B.; Datta, S.; Kavalieros, J.; Zhang, K. Integrated Nanoelectronics for the Future. *Nat. Mater.* **2007**, *6*, 810–812.

(2) Wei, J.; Jia, Y.; Shu, Q.; Gu, Z.; Wang, K.; Zhuang, D.; Zhang, G.; Wang, Z.; Luo, J.; Cao, A.; Wu, D. Double-Walled Carbon Nanotube Solar Cells. *Nano Lett.* **2007**, *7*, 2317–2321.

(3) Choi, W. B.; Chung, D. S.; Kang, J. H.; Kim, H. Y.; Jin, Y. W.; Han, I. T.; Lee, Y. H.; Jung, J. E.; Lee, N. S.; Park, G. S.; Kim, J. M. Fully Sealed, High-Brightness Carbon-Nanotube Field-Emission Display. *Appl. Phys. Lett.* **1999**, *75*, 3129–3131.

(4) Krasheninnikov, A. V.; Banhart, F. Engineering of nanostructured carbon materials with electron or ion beams. *Nat. Mater.* **2007**, *6*, 723–733.

(5) Sharma, H.; Agarwal, D. C.; Shukla, A. K.; Avasthi, D. K.; Vankar, V. D. Surface-Enhanced Raman scattering and Fluorescence Emission of Gold Nanoparticle–Multiwalled Carbon Nanotube Hybrids. *J. Raman Spectrosc.* **2013**, *44*, 12–20.

(6) Ma, P. C.; Tang, B. Z.; Kim, J.-K. Effect of CNT Decoration with Silver Nanoparticles on Electrical Conductivity of CNT-Polymer Composites. *Carbon* **2008**, *46*, 1497–1405.

(7) Pinto, H.; Jones, R.; Goss, J. P.; Briddon, P. R. Mechanisms of Doping Graphene. *Phys. Status Solidi A* **2010**, *207*, 2131–2136.

(8) Bissett, M. A.; Tsuji, M.; Ago, H. Mechanical Strain of Chemically Functionalized Chemical Vapor Deposition Grown Graphene. *J. Phys. Chem. C* **2013**, *117*, 3152–3159.

(9) Sharma, H.; Kaushik, V.; Girdhar, P.; Singh, V. N.; Shukla, A. K.; Vankar, V. D. Enhanced Electron Emission from Titanium Coated Multiwalled Carbon Nanotubes. *Thin Solid Films* **2010**, *518*, 6915–6920.

(10) Sharma, H.; Agarwal, D. C.; Sharma, M.; Shukla, A. K.; Avasthi, D. K.; Vankar, V. D. Tailoring of Structural and Electron Emission Properties of CNT Walls and Graphene Layers Using High-Energy Irradiation. *J. Phys. D: Appl. Phys.* **2013**, *46*, 315301–315308.

(11) Tapasztó, L.; Dobrik, G.; Nemes-Incze, P.; Vertesy, G.; Lambin, P.; Biró, L. P. Tuning the Electronic Structure of Graphene by Ion Irradiation. *Phys. Rev. B* **2008**, *78*, 233407–233410.

(12) Basiuk, V. A.; Kobayashi, K.; Kaneko, T.; Negishi, Y.; Basiuk, E. V.; Saniger-Blesa, J.-M. Irradiation of Single-Walled Carbon Nanotubes with High-Energy Protons. *Nano Lett.* **2002**, *2*, 789–791.

(13) Misra, A.; Tyagi, P. K.; Rai, P.; Mahopatra, D. R.; Ghatak, J.; Satyam, P. V.; Avasthi, D. K.; Misra, D. S. Axial Buckling and Compressive Behavior of Nickel-Encapsulated Multiwalled Carbon Nanotubes. *Phys. Rev. B* **2007**, *76*, 014108–014113.

(14) Mathew, S.; Chan, T. K.; Zhan, D.; Gopinadhan, K.; Barman, A. R.; Breese, M. B. H.; Dhar, S.; Shen, Z. X.; Venkatesan, T.; Thong, J.

T. L. The effect of layer number and substrate on the stability of graphene under MeV proton beam irradiation. *Carbon* **2011**, *49*, 1720−1726.
(15) Mathew, S.; Chan, T. K.; Zhan, D.; Gopinadhan, K.; Roy Barman, A.; Breese, M. B. H.; Dhar, S.; Shen, Z. X.; Venkatesan, T.; Thong, J. T. L. Mega-Electron-Volt Proton Irradiation on Supported and Suspended Graphene: A Raman Spectroscopic Layer Dependent Study. *J. Appl. Phys.* **2011**, *110*, 084309−084309.
(16) Nakajima, A.; Fujishima, A.; Hashimoto, K.; Watanabe, T. Preparation of Transparent Superhydrophobic Boehmite and Silica Films by Sublimation of Aluminum Acetylacetonate. *Adv. Mater.* **1999**, *11*, 1365−1368.
(17) Wang, Z.; Koratkar, N.; Ci, L.; Ajayan, P. M. Combined Micro-/Nanoscale Surface Roughness for Enhanced Hydrophobic Stability in Carbon Nanotube Arrays. *Appl. Phys. Lett.* **2007**, *90*, 143117−143113.
(18) Sharma, H.; Shukla, A. K.; Vankar, V. D. Influence of Fe Nanoparticles Diameters on the Structure and Electron Emission Studies of Carbon Nanotubes and Multilayer Graphene. *Mater. Chem. Phys.* **2013**, *137*, 802−810.
(19) Srivastava, S. K.; Shukla, A. K.; Vankar, V. D.; Kumar, V. Growth, structure and field emission characteristics of petal like carbon nano-structured thin films. *Thin Solid Films* **2005**, *492*, 124−130.
(20) Kaushik, V.; Shukla, A. K.; Vankar, V. D. Improved electron field emission from metal grafted graphene composites. *Carbon* **2013**, *62*, 337−345.
(21) Richard, G. F. Extraction of Emission Parameters for Large-Area Field Emitters, Using a Technically Complete Fowler−Nordheim-Type Equation. *Nanotechnology* **2012**, *23*, 095706.
(22) Kumar, A.; Avasthi, D. K.; Pivin, J. C.; Koinkar, P. M. Ordering of Fullerene and Carbon Nanotube Thin Films Under Energetic Ion Impact. *Appl. Phys. Lett.* **2008**, *92*, 221904−221906.
(23) Banhart, F.; Kotakoski, J.; Krasheninnikov, A. V. Structural Defects in Graphene. *ACS Nano* **2010**, *5*, 26−41.
(24) Misra, A.; Tyagi, P. K.; Rai, P.; Misra, D. S.; Ghatak, J.; Satyam, P. V.; Avasthi, D. K. Reorientation of the Crystalline Planes in Confined Single Crystal Nickel Nanorods Induced by Heavy Ion Irradiation. *Appl. Phys. Lett.* **2006**, *89*, 091907−091909.
(25) Dresselhaus, M. S.; Jorio, A.; Saito, R. Characterizing Graphene, Graphite, and Carbon Nanotubes by Raman Spectroscopy. *Annu. Rev. Condens. Matter Phys.* **2010**, *1*, 89−08.
(26) Sharma, H.; Shukla, A. K.; Vankar, V. D. Structural Modifications and Enhanced Raman Scattering from Multiwalled Carbon Nanotubes Grown on Titanium Coated Silicon Single Crystals. *Thin Solid Films* **2012**, *520*, 1902−1908.
(27) Cronin, S. B.; Swan, A. K.; Ünlü, M. S.; Goldberg, B. B.; Dresselhaus, M. S.; Tinkham, M. Measuring the Uniaxial Strain of Individual Single-Wall Carbon Nanotubes: Resonance Raman Spectra of Atomic-Force-Microscope Modified Single-Wall Nanotubes. *Phys. Rev. Lett.* **2004**, *93*, 167401.
(28) Cronin, S. B.; Swan, A. K.; Ünlü, M. S.; Goldberg, B. B.; Dresselhaus, M. S.; Tinkham, M. Resonant Raman spectroscopy of individual metallic and semiconducting single-wall carbon nanotubes under uniaxial strain. *Phys. Rev. B* **2005**, *72*, 035425.
(29) Krasheninnikov, A. V.; Nordlund, K. Ion and Electron Irradiation-Induced Effects in Nanostructured Materials. *J. Appl. Phys.* **2010**, *107*, 071301−071370.
(30) Young, R. J.; Gong, L.; Kinloch, I. A.; Riaz, I.; Jalil, R.; Novoselov, K. S. Strain Mapping in a Graphene Monolayer Nanocomposite. *ACS Nano* **2011**, *5*, 3079−3084.
(31) Ni, Z. H.; Wang, H. M.; Ma, Y.; Kasim, J.; Wu, Y. H.; Shen, Z. X. Tunable Stress and Controlled Thickness Modification in Graphene by Annealing. *ACS Nano* **2008**, *2*, 1033−1039.
(32) Yakobson, B. I.; Brabec, C. J.; Bernholc, J. Nanomechanics of Carbon Tubes: Instabilities Beyond Linear Response. *Phys. Rev. Lett.* **1996**, *76*, 2511−2514.
(33) Wu, G.; Zhou, J.; Dong, J. Raman Modes of the Deformed Single-Wall Carbon Nanotubes. *Phys. Rev. B* **2005**, *72*, 115411−115421.
(34) Wang, S.; Zhang, Y.; Abidi, N.; Cabrales, L. Wettability and Surface Free Energy of Graphene Films. *Langmuir* **2009**, *25*, 11078−11081.
(35) Wenzel, R. N. Resistance of Solid Surfaces to Wetting by Water. *Ind. Eng. Chem.* **1936**, *28*, 988−994.
(36) Rafiee, J.; Rafiee, M. A.; Yu, Z.-Z.; Koratkar, N. Superhydrophobic to Superhydrophilic Wetting Control in Graphene Films. *Adv. Mater.* **2010**, *22*, 2151−2154.
(37) Carroll, D. L.; Redlich, P.; Ajayan, P. M.; Charlier, J. C.; Blase, X.; De Vita, A.; Car, R. Electronic Structure and Localized States at Carbon Nanotube Tips. *Phys. Rev. Lett.* **1997**, *78*, 2811−2814.